

# Open-world Hand-Object Interaction Video Generation Based on Structure and Contact-aware Representation

Haodong Yan<sup>1</sup> Hang Yu<sup>1</sup> Zhide Zhong<sup>1</sup> Weilin Yuan<sup>1</sup> Xin Gong<sup>1</sup> Zehang Luo<sup>1</sup>  
 Chengxi Heyu<sup>1</sup> Junfeng Li<sup>1</sup> Wenxuan Song<sup>1</sup> Shunbo Zhou<sup>2</sup> Haoang Li<sup>1</sup>

<sup>1</sup>The Hong Kong University of Science and Technology (Guangzhou) <sup>2</sup>Huawei Cloud

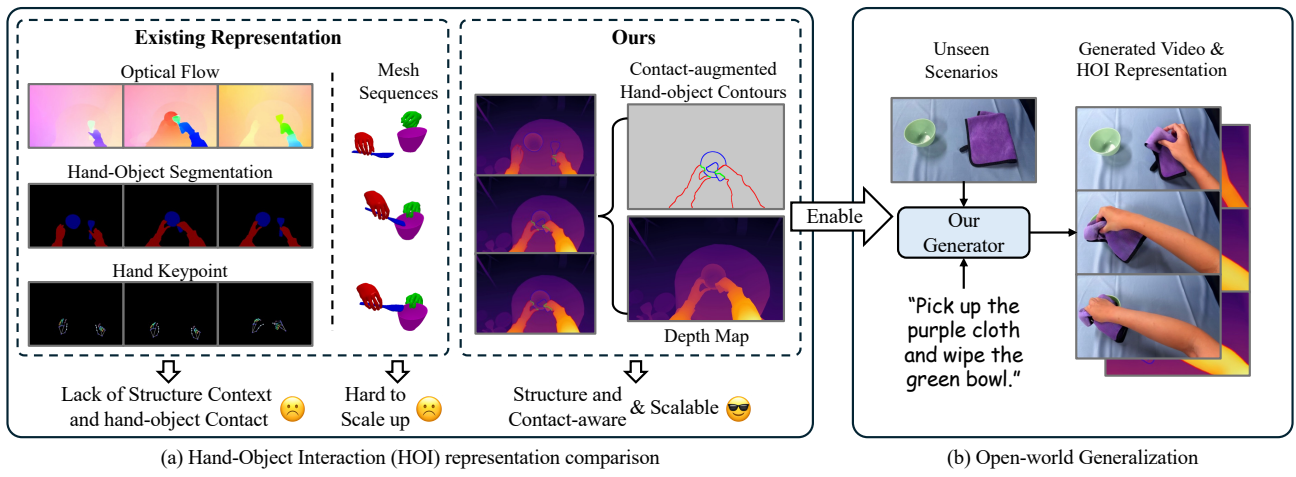


Figure 1. Overview of our structure and contact-aware representation and its enabled open-world generalization. (a) Prior HOI representations lack either scalability (e.g., 3D mesh) or crucial contact/structure cues (e.g., optical flow or segmentation). Our approach resolves this dilemma with a representation composed of two scalable and complementary components: 1) contact-augmented hand-object contours for capturing the contact region and hand-object spatial localization, and 2) depth maps offering holistic structure context. (b) Our structure and contact-aware representation acts as an additional interaction-oriented generative supervision signal. By learning to jointly generate videos and our representation at a large scale, our model captures interaction patterns consistent with physical constraints, enabling strong generalization to complex open-world interactions, even with unseen non-rigid objects.

## Abstract

Generating realistic hand-object interactions (HOI) videos is a significant challenge due to the difficulty of modeling physical constraints (e.g., contact and occlusion between hands and manipulated objects). Current methods utilize HOI representation as an auxiliary generative objective to guide video synthesis. However, there is a dilemma between 2D and 3D representations that cannot simultaneously guarantee scalability and interaction fidelity. To address this limitation, we propose a structure and contact-aware representation that captures hand-object contact, hand-object occlusion, and holistic structure context without 3D annotations. This interaction-oriented and scalable supervision signal enables the model to learn fine-grained interaction physics and generalize to open-world scenarios. To fully exploit the proposed representation, we introduce a

joint-generation paradigm with a share-and-specialization strategy that generates interaction-oriented representations and videos. Extensive experiments demonstrate that our method outperforms state-of-the-art methods on two real-world datasets in generating physics-realistic and temporally coherent HOI videos. Furthermore, our approach exhibits strong generalization to challenging open-world scenarios, highlighting the benefit of our scalable design. Our project page is <https://hgzn258.github.io/SCAR/>.

## 1. Introduction

Achieving a deep understanding and enabling realistic synthesis of this complex hand-object interaction (HOI) is a key challenge in computer vision. This domain has wide-

ranging applications in robotic learning [16, 45], augmented reality [15, 32], and human behavior analysis [7, 11]. A particularly challenging frontier for this task is HOI video generation. Conditioned on an observed image and a task description, the goal is to synthesize a video sequence of hands manipulating objects with physics-realistic interaction and temporally coherent motion. Although recent video generation models [13, 34, 36, 37, 39, 43] have made progress in photorealism and visual fidelity, their success does not readily transfer to the nuanced domain of HOI generation. The lack of specific inductive biases (e.g., hand-object contact and holistic structure) causes these general-purpose models to often fail on physics realism.

One line of work [24, 45] attempts to tackle this problem by leveraging an HOI representation that explicitly models physical interaction cues as an auxiliary objective. Despite this advance, the design of the HOI representation presents a dilemma between scalability and interaction fidelity (see Fig. 1(a)). Scalable 2D representations such as optical flow [20, 36], hand-object segmentation [24, 44], and hand keypoint [45] lack a holistic structure context and a hand-object contact region. Conversely, 3D mesh sequences [4, 6, 17, 30] with complete structure context suffer from poor scalability due to costly 3D annotations. In addition, these approaches [20, 24, 36, 44, 45] follow a multi-stage paradigm, where each stage is trained with ground-truth inputs yet conditioned on predictions from the previous stage at inference, causing accumulated errors that degrade both physics realism and visual quality [20, 21, 38].

To address the aforementioned scalability-fidelity dilemma, we introduce a novel representation whose overall design is depicted in Fig. 1(a). It consists of two complementary and scalable components: 1) a contact-augmented hand-object contour that explicitly captures hand-object contact and spatial localization, and 2) a depth map that provides the holistic structure context. This structure and contact-aware representation thus serves as a scalable and interaction-oriented supervisory signal. It guides the model to learn interaction patterns consistent with physical constraints, thereby promoting both physics-realistic generation and open-world generalization (see Fig. 1(b)).

Briefly, we generate the above representation as follows. To create the contact-augmented hand-object contour, we first use a vision-language model (VLM) [1] with a sophisticated Chain-of-Thought (CoT) [41] prompt to ground hands and objects. Subsequently, we leverage SAM2 [33] to extract and propagate hand-object masks, from which we derive an elegant and powerful proxy for the hand-object contact region by computing the intersection of their dilated contours. For the second component, the depth map is obtained from a video-consistent depth estimator [5].

Based on the above representation, we propose a joint-

generation paradigm as shown in Fig. 3. Different from mainstream multi-stage approaches [20, 24, 36, 44, 45], our method generates proposed HOI representations and videos simultaneously to mitigate error accumulation. This paradigm is enabled by a hierarchical joint denoiser, which learns the joint distribution between videos and their structure and contact-aware representations through two cascaded modules: 1) a *Shared Semantics* module that captures shared, modality-invariant semantics by enforcing alignment via an explicit regularization loss on hidden states, and 2) a *Specialized Details* module that removes this constraint to capture unique, modality-specific characteristics. By integrating the above techniques, our method achieves physics-realistic HOI video generation. To summarize, our contributions are as follows:

- We propose a structure and contact-aware representation as a scalable and interaction-oriented supervisory signal that guides the model to capture fine-grained interaction physics. We curate this representation for over 100k HOI videos, facilitating large-scale training.
- We introduce a joint-generation paradigm with a share-and-specialization strategy that generates proposed HOI representations and videos simultaneously, mitigating multi-stage error accumulation.
- Extensive experiments demonstrate our method generates physics-realistic HOI videos, surpassing state-of-the-art methods on two real-world datasets and showing strong generalization to open-world scenarios.

## 2. Related Work

### 2.1. Hand-Object Interaction Representation

Hand-object interaction (HOI) representation aims to capture both the individual dynamics of hands and objects and their physical correlations (e.g., contact and occlusion). In HOI generation and prediction tasks [4, 6, 17, 29, 46], interactions are commonly represented as sequences of MANO parameters [35] or 3D hand keypoints, along with object meshes or point clouds. While offering fine-grained structure detail for physical realism, these high-fidelity representations lack explicit signals for crucial interaction semantics, such as physical contact. To bridge this gap, some works further extract interaction-centric features directly from this 3D data. HOI-GEN [15] and ManiVideo [30] introduce occlusion-aware topology maps as HOI representation, which improves depth and occlusion consistency and enriches spatial control. Another line of work [10, 19, 22, 25, 47] utilizes the contact map as the primary HOI representation. These methods explicitly model regions of physical interaction between the hand and object, offering a focused representation for contact semantics. However, these representations with high interaction fidelity rely on expensive 3D annotations (e.g., motion capture) that are hard to

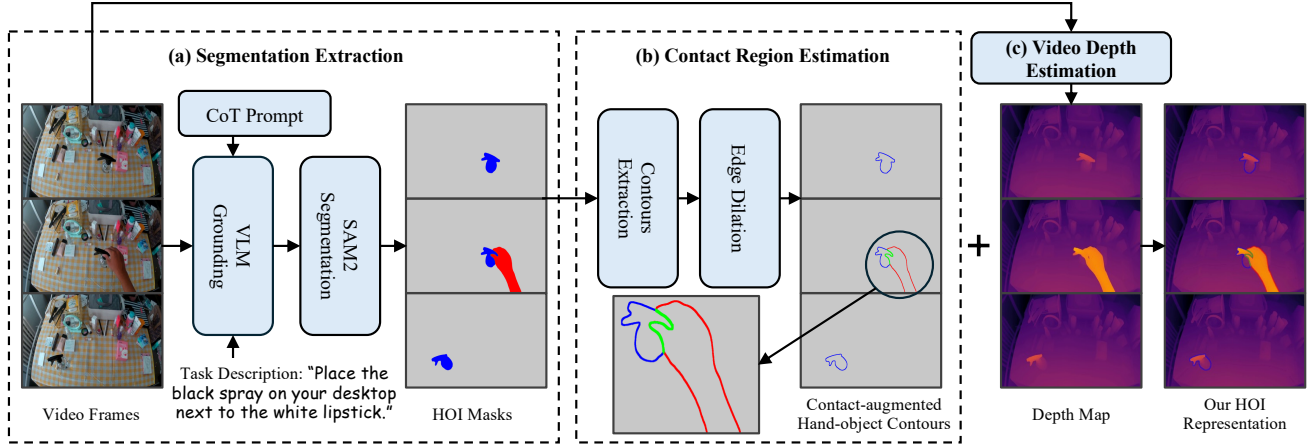


Figure 2. Overview of our structure and contact-aware representation curation pipeline. It begins with (a) **Segmentation Extraction**, where a CoT-guided VLM grounds hand and object from the input RGB video, and SAM2 generates HOI masks. Next, (b) **Contact Region Estimation** produces the final contact-augmented hand-object contours by computing a contact region from the intersection of the dilated hand and object contours. In parallel, (c) **Video Depth Estimation** generates a dense depth map sequence for holistic structure. Finally, these contact-augmented hand-object contours are alpha-blended onto the depth maps to form the final HOI representation.

scale up. To address this issue, an alternative approach leverages scalable motion representations like overlapped masks [24, 44], optical flow [20, 36], or 2D hand keypoints [2, 45]. Despite their scalability, these representations fail to capture hand-object contact regions and a holistic structure context in the scene. In contrast, we introduce a structure and contact-aware representation that encodes hand-object contact, hand-object spatial localization, and holistic structure context without 3D annotations.

## 2.2. Hand-Object Interaction Video Generation

The synthesis of the human-object interaction (HOI) has recently benefited from significant advances in video generation [23, 37, 39, 43] with powerful Diffusion Transformer (DiT) architectures [31]. Current HOI video generation research can be broadly categorized into representation-conditioned and task-guided settings. The former methods [8, 30, 40, 42] generate HOI videos by conditioning on pre-existing HOI representations. However, these methods face significant input constraints, as their reliance on control signals must be manually predefined or extracted from a driving video. In contrast, the task-guided methods [9, 24, 45] generate HOI videos conditioned on textual commands, which are more readily available and practical for real-world applications. For example, VPP [16] directly fine-tunes SVD [3] on HOI data to adapt the domain. Mask2V [24] first predicts an interaction trajectory represented by a sequence of masks, and then uses this trajectory to guide the final video generation. Taste-Rob [45] first generates a coarse video to extract an initial hand pose sequence. This sequence is then refined by a motion diffusion model and used as a condition for the final video

generation.

However, existing methods struggle with physics realism and the generalization ability to open-world scenarios, primarily due to the representation dilemma (Sec. 2.1). In addition, these approaches often rely on a multi-stage paradigm, which is susceptible to error accumulation. In contrast, our work employs a joint-generation paradigm to mitigate error accumulation and capture the inherent correlation between HOI representation and video.

## 3. Method

In this section, we first introduce our structure and contact-aware HOI representation in Sec. 3.1. Then, we detail our joint-generation paradigm in Sec. 3.2 to generate the proposed HOI representation and videos simultaneously.

### 3.1. Structure and Contact-aware Representation

As illustrated in Fig. 1(a), our representation is formed by alpha-blending two scalable and complementary components: (1) contact-augmented contours that encode hand-object contact and hand-object spatial localization, and (2) depth maps providing holistic structure context. We chose sparse contours instead of dense masks to capture hand-object spatial localization because sparse contours preserve the depth map during alpha-blending, while dense masks tend to obscure this critical information. The full curation pipeline is detailed below.

**Segmentation Extraction.** As depicted in Fig. 2(a), we adopt a grounding-and-tracking pipeline to obtain hand and object masks. Specifically, we first localize the hand and object using a large VLM [1] prompted with Chain-of-Thought (CoT) reasoning. The CoT prompt guides the

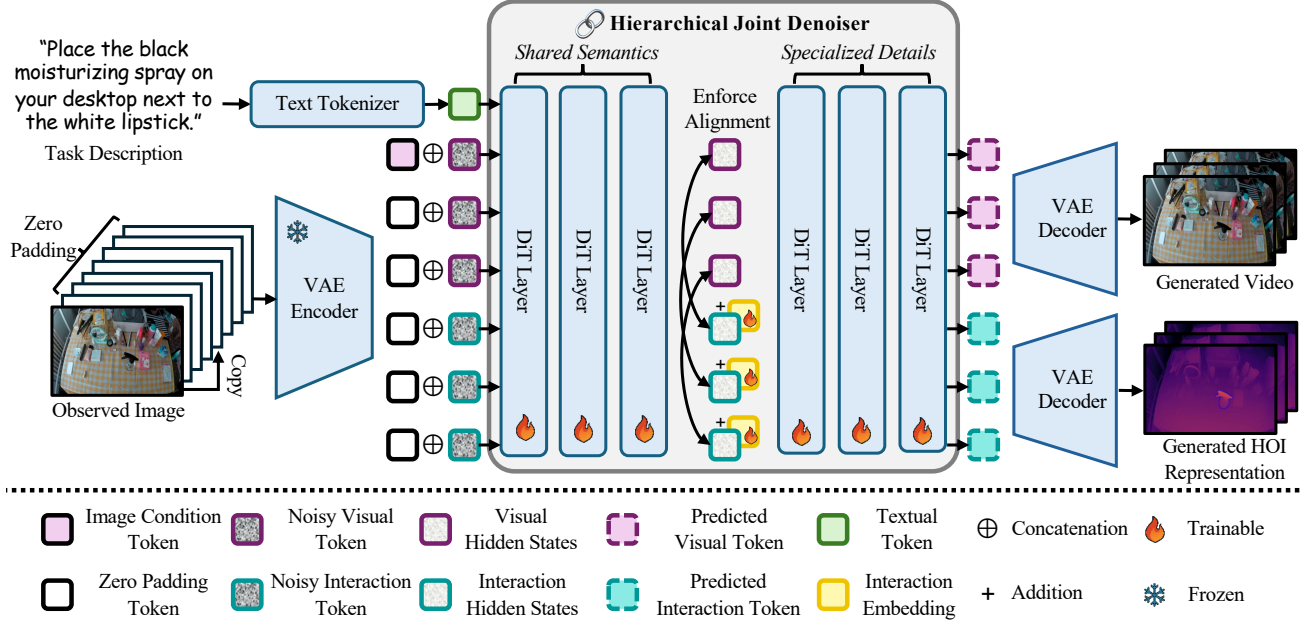


Figure 3. The joint-generation paradigm of our method. Given an observed image and a task description, our framework jointly generates a video and its corresponding HOI representation. The core technical novelty lies in the **Hierarchical Joint Denoiser** that co-denoises visual and interaction tokens within a unified latent space. First, the *Shared Semantics* module enforces cross-modal consistency via an alignment loss (maximizing cosine similarity) to capture shared semantics like spatial layout and temporal dynamics. Then, the *Specialized Details* module adds a learnable interaction embedding to capture modality-specific details. Finally, the denoised predicted visual and interaction tokens are passed through the VAE decoder to reconstruct both outputs.

VLM to sequentially verify textual intent, visual interaction cues, and temporal motion, enabling more reliable grounding than specialized detectors [26], especially for open-vocabulary objects and complex scenes involving distractors. Details of VLM-based grounding are provided in the supplementary material. Then, we use the grounded bounding boxes to prompt SAM2 [33], which extracts and propagates them into per-frame hand and object masks. To guarantee the final annotation quality, this automated process was followed by a manual verification stage, where human annotators review and correct the generated masks.

**Contact Region Estimation.** Given the hand and object masks, we estimate the hand-object contact region by identifying areas where their boundaries exhibit close spatial proximity (see Fig. 2(b)). Specifically, we first convert these masks into thin contours, denoted as  $E_h$  and  $E_o$ . We then estimate hand-object contact regions by dilating the hand with a fixed radius,  $r_h$ , and the object with a scale-adaptive radius,  $r_o$ , to robustly handle its significant scale variations. To ensure robustness to extreme object scales,  $r_o$  is calculated proportionally to the diagonal length of its bounding box  $L$  and constrained in a reasonable range  $[r_{\min}, r_{\max}]$ :

$$r_o = \min(r_{\max}, \max(r_{\min}, \beta \cdot L)). \quad (1)$$

Here,  $\beta$  is a proportional coefficient. The hand-object contact region,  $C$ , is defined as the intersection of these dilated

contours:

$$C = \text{dilate}(E_h, r_h) \cap \text{dilate}(E_o, r_o). \quad (2)$$

This simple yet highly scalable proxy provides reliable estimates of contact regions. The effectiveness of this estimated contact region is demonstrated in Sec. 4.4.

**Video Depth Estimation.** To complement our HOI representation with 3D structure context, we incorporate per-frame depth maps (see Fig. 2(c)). We generate these using a state-of-the-art video-consistent depth estimation model [5], which provides crucial information on relative depth ordering. While such models are often scale-ambiguous, their estimated relative structure is highly reliable. Our curated representation leverages this robust signal, providing a scalable 3D structure context independent of absolute scale.

### 3.2. Joint Generation of Video and Representation

To fully exploit our representation without multi-stage error accumulation, we propose a novel joint-generation paradigm (see Fig. 3). By compelling the model to simultaneously generate both HOI representation and the RGB video from a unified latent space, we provide an additional interaction-oriented supervisory signal, guiding the model to generate physics-realistic interactions.

**Unified Latent Space.** We adopt a 3D VAE to encode the RGB video ( $V_{\text{RGB}}$ ) and the HOI representation ( $V_{\text{HOI}}$ ) into a unified latent space, yielding visual tokens ( $X_{\text{RGB}}$ ) and interaction tokens ( $X_{\text{HOI}}$ ). The video-like structure of our HOI representation enables this joint encoding. Our model operates on this unified space by concatenating these tokens  $X_{\text{RGB}}$  and  $X_{\text{HOI}}$  into a single sequence  $Z = (X_{\text{RGB}} \oplus X_{\text{HOI}})$ . During training,  $Z$  is corrupted to  $Z_t = \sqrt{\bar{\alpha}_t} Z + \sqrt{1 - \bar{\alpha}_t} \varepsilon$ , and our denoiser is trained to predict the added noise  $\hat{\varepsilon}$  from  $Z_t$ . During inference, the denoiser reverses this process from pure noise  $Z_T$  to recover the clean tokens  $Z_0$ , which are then decoded by the VAE to jointly generate the RGB video  $\hat{V}_{\text{RGB}}$  and its corresponding HOI representation  $\hat{V}_{\text{HOI}}$ .

**Hierarchical Joint Denoiser.** We introduce a hierarchical joint denoiser, built upon a Diffusion Transformer (DiT) backbone, to co-denoise visual and interaction tokens, conditioned on a task description and an observed image (as shown in Fig. 3). The core of this denoiser is a novel share-and-specialization strategy. This strategy is motivated by the dual nature of these two modalities: they are inherently semantically coupled, yet each exhibits distinct modality-specific characteristics. We implement this strategy by partitioning the DiT layers into two cascaded modules.

Specifically, the *Shared Semantic* module (layers 1 to  $k^*$ ) enforces cross-modal consistency via our alignment loss,  $L_{\text{align}}$ . This loss compels the hidden states of both the visual and interaction streams to align by explicitly maximizing the cosine similarity between their hidden states from layer  $k^*$ :

$$L_{\text{align}} = \sum_{m=1}^S \left( 1 - \frac{H_{k^*}^m \cdot H_{k^*}^{S+m}}{\|H_{k^*}^m\| \|H_{k^*}^{S+m}\|} \right), \quad (3)$$

where  $H_{k^*}^m$  is the hidden state for the  $m$ -th visual token and  $H_{k^*}^{S+m}$  is the hidden state for the corresponding  $m$ -th interaction token. Here,  $S$  is the total number of visual tokens. This forced alignment compels the module to learn the shared interaction semantics between video and HOI representation. Starting from layer  $k^*+1$ , the *Specialized Details* module introduces a learnable interaction embedding,  $d_{\text{HOI}}$ . This embedding is added exclusively to the interaction token hidden states output by layer  $k^*$  (i.e.,  $\tilde{H}_{k^*}^m = H_{k^*}^m + d_{\text{HOI}}$  for  $m > S$ ), before the subsequent DiT layers process them. This injection introduces a modality-specific bias that encourages the network to capture the unique characteristics required for each distinct stream.

In addition, across both modules, each DiT layer adopts two architectural modifications for better adaptation to interaction tokens. For one thing, we assign identical positional encodings to the visual and interaction tokens sharing the same spatio-temporal position, thereby explicitly encoding their correspondence. Before the self-attention operation in layer  $k$ , the hidden states from the previous layer

$H_{k-1}$  are modulated by these encodings, yielding the modulated tokens  $P_k^m$ :

$$P_k^m = \begin{cases} H_{k-1}^m + p^m, & \text{if } m \leq S, \\ H_{k-1}^m + p^{m-S}, & \text{if } m > S. \end{cases} \quad (4)$$

For another, we integrate lightweight LoRA modules [14] into the self-attention projection matrices ( $\mathbf{W}_Q, \mathbf{W}_K, \mathbf{W}_V$ ) for efficiency. To adapt the model for HOI generation while retaining its pre-trained visual knowledge, the LoRA update is applied selectively at the output stage using a binary mask. For each projection matrix  $\mathbf{W}_z$  (where  $z \in \{\mathcal{Q}, \mathcal{K}, \mathcal{V}\}$ ) and its corresponding low-rank adaptation LoRA $_z(\cdot)$ , the projected output  $\mathbf{X}_z^*$  for the sequence  $P_k$  is given by:

$$\mathbf{X}_z^* = P_k \mathbf{W}_z + \gamma \cdot \text{diag}(\mathbf{M}) \text{LoRA}_z(P_k). \quad (5)$$

Here,  $\gamma$  is a scaling factor and  $\mathbf{M} \in \{0, 1\}^{2S}$  is a binary mask (converted to its diagonal form) that activates LoRA updates only for interaction tokens.

**Training Loss.** Our composite loss combines the alignment loss ( $L_{\text{align}}$ ) alongside diffusion losses for visual tokens ( $L_{\text{RGB}}$ ) and interaction tokens ( $L_{\text{HOI}}$ ):

$$L = L_{\text{RGB}} + \lambda_{\text{HOI}} L_{\text{HOI}} + \lambda_{\text{align}} L_{\text{align}}. \quad (6)$$

Here,  $L_{\text{RGB}}$  and  $L_{\text{HOI}}$  can be formulated based on different prediction targets, such as the original noise [12] or velocity [27]. The terms  $\lambda_{\text{HOI}}$  and  $\lambda_{\text{align}}$  balance the diffusion loss for interaction tokens and the alignment loss.

## 4. Experiments

### 4.1. Experimental Setup

**Datasets.** We conduct experiments on Taste-Rob [45] and Taco [28] datasets. Taste-Rob is a large-scale fixed-view HOI dataset consisting of 100,856 videos, each paired with a manually annotated task description. This dataset features both single-hand and double-hand interactions, covering a diverse range of action categories (e.g., grasping, lifting, rotating), object types, and scene layouts. We follow Taste-Rob [45] to split training and test sets.

We also conduct experiments on the Taco dataset. This dataset comprises 2,317 videos of double-hand interactions from both egocentric and third-person viewpoints. For our experiments, we only use the videos captured from the egocentric perspective, which inherently involves significant camera motion and complex background changes. We split the data into training (90%) and testing (10%) sets according to the dataset’s triplet (action, tool, target object) categorization, ensuring each triplet is randomly split.

**Evaluation Criteria.** We employ a set of video generation metrics from VBench [18] to assess three key aspects: (1)

Table 1. Quantitative comparison with state-of-the-art methods on the Taste-Rob [45] and Taco [28] datasets. All metrics are from VBench [18] and higher is better ( $\uparrow$ ). Our method consistently outperforms prior work across all categories. The best results are in **bold**, while the second best are underlined.

Method	Taste-Rob [45]								Taco [28]							
	Video Quality		Image Align.		Text. Align.		Overall		Video Quality		Image Align.		Text. Align.		Overall	
	SC $\uparrow$	IQ $\uparrow$	ISC $\uparrow$	IBC $\uparrow$	VCS $\uparrow$	TS $\uparrow$	SC $\uparrow$	IQ $\uparrow$	ISC $\uparrow$	IBC $\uparrow$	VCS $\uparrow$	TS $\uparrow$	SC $\uparrow$	IQ $\uparrow$	ISC $\uparrow$	IBC $\uparrow$
CogVideoX [43]	0.959	0.688	0.955	0.954	0.187	8.959	0.895	0.665	0.933	0.942	0.182	8.511				
Wan2.1 [37]	0.943	<u>0.700</u>	0.947	0.939	0.185	8.897	0.905	<u>0.717</u>	0.933	0.947	0.189	8.792				
FLOVD [20]	0.941	0.691	0.949	0.956	0.189	8.888	0.903	0.686	0.927	0.947	0.177	8.619				
SCAR <sub>C</sub> (our)	<b>0.964</b>	0.696	<u>0.960</u>	<b>0.959</b>	<u>0.193</u>	<u>9.043</u>	<b>0.916</b>	0.698	<b>0.951</b>	<b>0.954</b>	<u>0.187</u>	<u>8.793</u>				
SCAR <sub>W</sub> (our)	<u>0.961</u>	<b>0.709</b>	<b>0.961</b>	<u>0.958</u>	<b>0.194</b>	<b>9.084</b>	<u>0.912</u>	<b>0.728</b>	<u>0.948</u>	<u>0.952</u>	<b>0.191</b>	<b>8.899</b>				

**Video Quality**, evaluated using *subject consistency* (SC) and *imaging quality* (IQ), (2) **Image-to-Video Alignment**, evaluated using *i2v subject consistency* (ISC) and *i2v background consistency* (IBC) to assess consistency with the observed image, and (3) **Text-to-Video Alignment**, evaluated using the *viclip score* (VCS) for consistency with the task description. Finally, we report the weighted *total score* (TS), which integrates these metrics based on the coefficients defined in VBench [18].

**Implementation Details.** To demonstrate the versatility of our method, we adapt our approach to two mainstream pre-trained video diffusion models (VDMs): CogVideoXI2V-5B and Wan2.1I2V-14B. We denote these two instantiations as SCAR<sub>C</sub> and SCAR<sub>W</sub>, respectively. We preserve the core architecture of the base VDMs, including their original VAE latent space, number of DiT layers, and hidden state dimensions. For video generation length, we set the sequence length to 17 frames for the Taste-Rob [45] and 25 frames for the Taco [28]. For SCAR<sub>C</sub>, we set the LoRA dimension to 128 and apply an alignment loss to the hidden states of the 12th DiT layer. For SCAR<sub>W</sub>, the LoRA dimension is increased to 256, and the alignment loss is applied to the 12th DiT layer. For both instantiations, the weights for the HOI diffusion loss,  $\lambda_{\text{HOI}}$ , and the alignment loss,  $\lambda_{\text{align}}$ , are consistently set to 1.0 and 0.1, respectively.

## 4.2. Comparisons with State-of-the-art Methods

**Methods for Comparison.** We compare our two instantiations, SCAR<sub>C</sub> and SCAR<sub>W</sub>, against state-of-the-art video generation models. These baselines comprise two categories. First, we conduct a direct evaluation against their own underlying backbones, the general-purpose models CogVideoX [43] and Wan2.1 [37]. Second, we compare against FLOVD [20], a representative two-stage method. To maintain fairness (especially against our SCAR<sub>C</sub>), we specifically fine-tune its CogVideoX-based instead of SVD-based instantiation. To ensure a fair comparison, all methods (both our instantiations and the baselines) are fine-tuned

on the same dataset splits and initialized from the same pre-trained model checkpoints. Further implementation details for all methods are provided in the supplementary material.

**Results.** As depicted in Fig. 4, general I2V models without HOI representation, CogVideoX, often struggle with physics realism, generating videos with distorted hands and objects, and unrealistic contact. This observation is consistent with their lower video quality scores (SC and IQ) reported in Tab. 1. Although Wan2.1 produces higher video quality, its failure to align with the task description (e.g., failing to brush the bowl as the task description) directly results in a low text-to-video alignment score (VCS). The two-stage model FLOVD suffers from error propagation, where inaccuracies from the initial optical flow (visualized in Fig. 5) are compounded in the second stage, resulting in temporal inconsistencies and hallucinated objects (e.g., the red object). This failure to maintain object identity is quantitatively reflected in its poor performance on the image-to-video alignment metrics (particularly ISC). In contrast, our SCAR framework generates physics-realistic and temporally coherent videos that execute the “brushing” action (see last two rows in Fig. 4), achieving superior performance across all metrics in Tab. 1. The high fidelity of the generated HOI representation (see Fig. 5) demonstrates that the model has captured the underlying physical constraints and interaction patterns for physics-realistic video synthesis. Notably, consistent performance gains of both SCAR<sub>C</sub> and SCAR<sub>W</sub> over baselines further demonstrate the versatility of our approach. Additionally, we provide more qualitative comparisons (including results on the Taste-Rob [45] dataset) in the supplementary material.

## 4.3. Generalization to Open-world Scenarios

To evaluate the open-world generalization of our method beyond the closed-set environments, we collect a new benchmark of 200 challenging open-world samples. Each sample consists of a task description and an image containing unseen target objects. Without loss of generality, we use

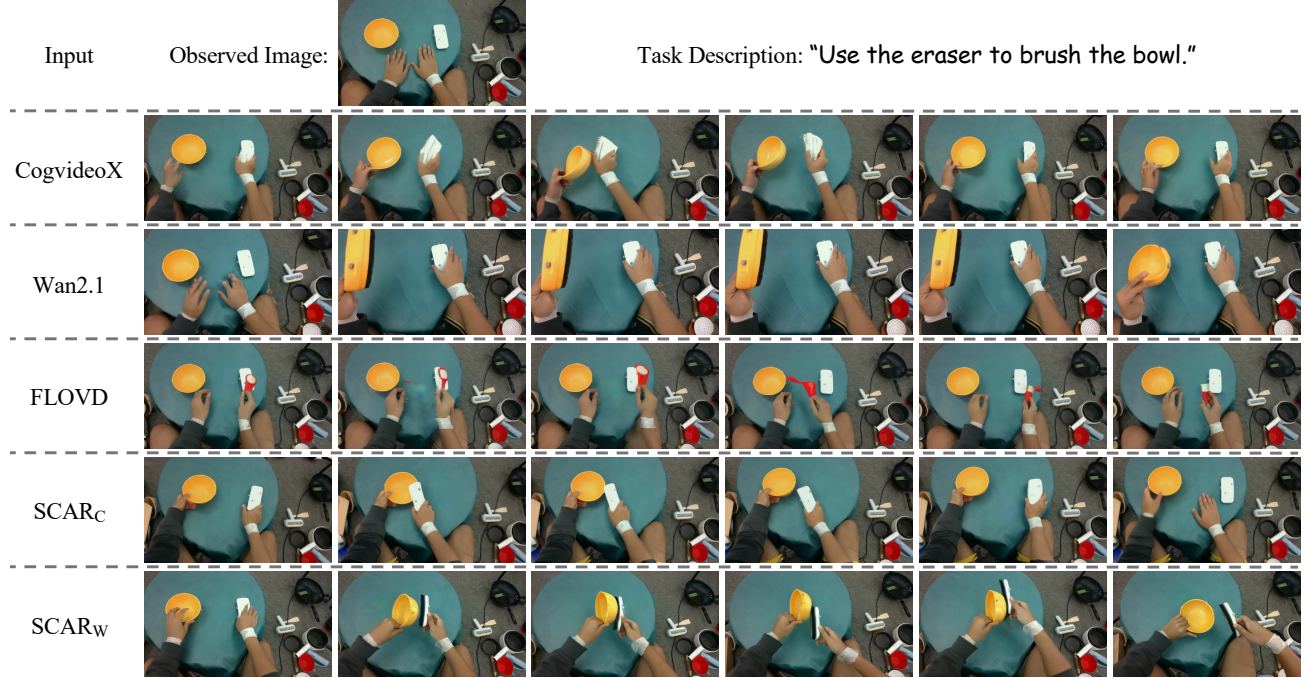


Figure 4. Qualitative comparison with state-of-the-art methods on Taco [28] dataset. CogVideoX [43] produces distorted hands and implausible contact. Wan2.1 [37] fails to generate the semantically correct action described in the task description. The two-stage FLOVD [20] suffers from error propagation, where inaccurate initial optical flow results in hallucination (a red object suddenly appearing). In contrast, our SCAR generates physics-realistic, temporally coherent videos by jointly generating our proposed HOI representation. Please refer to the supplementary video for better illustration. Experimental results on the Taste-Rob [45] are also available in the supplementary material.

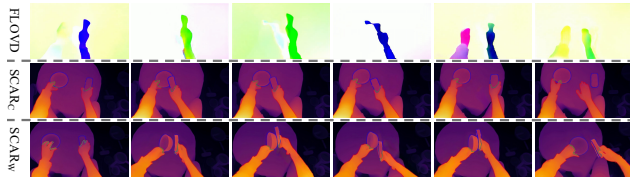


Figure 5. Qualitative comparison of generated HOI representations corresponding to Fig. 4. The optical flow generated by FLOVD [20] is noisy and inaccurate, which leads to the error propagation seen in the final video. In contrast, our jointly generated representation embodies consistent structural and contact cues, indicating that the model captures physical interaction patterns.

our SCAR<sub>W</sub> trained on the Taste-Rob [45] dataset for this evaluation.

As demonstrated in Fig. 6, we present a representative qualitative comparison in a challenging open-world scenario, where the entire scene consists of unseen objects (e.g., the semi-transparent cup, carrot, green bowl) that act as complex distractors for one another. All baseline methods (CogVideoX [43], Wan2.1 [37], FLOVD [20]) exhibit significant hand-object distortion, temporal inconsistencies, and physically implausible contact. Furthermore, their generated videos often fail to align with the task description.

Specifically, CogVideoX places the carrot into the green bowl instead of the “glass cup”. Wan2.1 exhibits poor object grounding, picking up the wrong item entirely. FLOVD fails to follow the precise instruction, moving the carrot “towards” rather than “into” the cup. These qualitative failures are corroborated by relatively low metrics (see the supplementary material). These baseline methods, even with large-scale finetuning, still struggle with generalization as they have difficulty capturing complex interaction physics. By comparison, our SCAR generates physics-realistic and temporally coherent videos in challenging open-world scenarios, achieving superior performance across all metrics. This success highlights that our method captures interaction patterns consistent with physical constraint by learning to jointly predict the video and our structure and contact-aware representation. We provide more qualitative comparisons in the supplementary material.

#### 4.4. Analysis of HOI Representation Design

In this subsection, we evaluate the effectiveness of our HOI representation design by comparing our full model against two categories of variants (see Tab. 2). Without loss of generality, all experiments for this analysis are conducted on the Taco [28] dataset, using SCAR<sub>C</sub> as our full model.

**Comparison with Existing Representation.** The first cat-

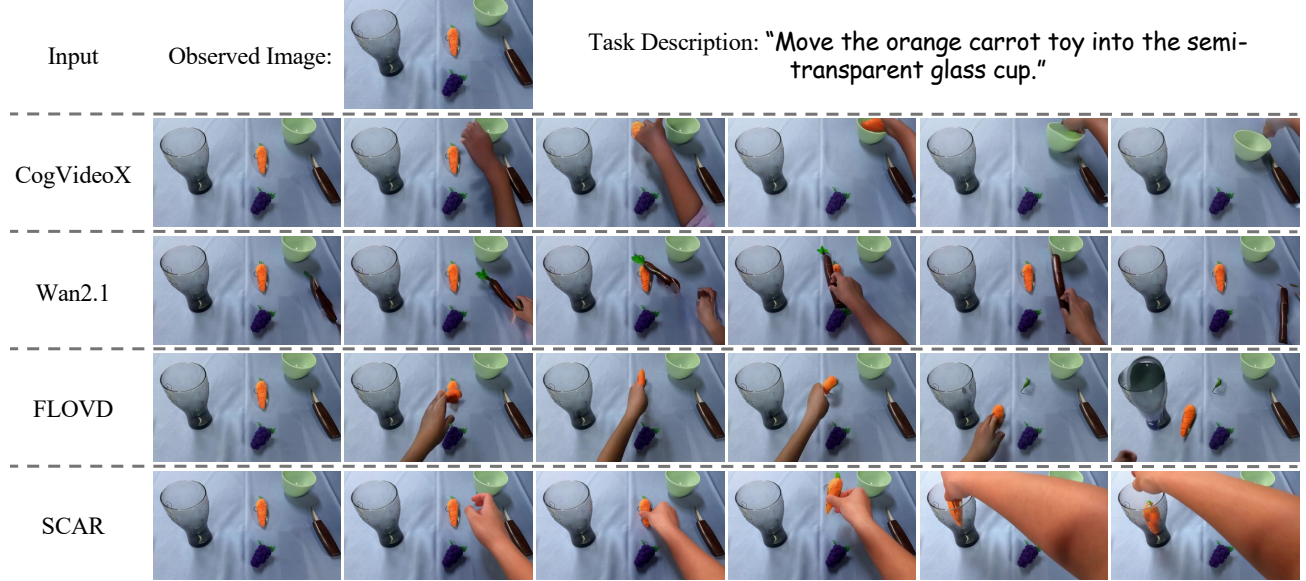


Figure 6. Qualitative comparison on a challenging open-world task. CogVideoX [43], Wan2.1 [37], and FLOVD [20] fail to follow the task description and produce physically implausible interactions. In contrast, our SCAR generates a physics-realistic, coherent video that correctly executes the challenging task involving unseen target objects and distractors.

Table 2. Quantitative comparison of different HOI representations. For all metrics, higher is better ( $\uparrow$ ). The best results are in **bold**.

HOI Rep.	Video Quality		Image Align.		Text Align.
	SC $\uparrow$	IQ $\uparrow$	ISC $\uparrow$	IBC $\uparrow$	VCS $\uparrow$
OF	0.889	0.660	0.935	0.942	0.177
HOM	0.903	0.689	0.939	0.945	0.181
DM	0.889	0.682	0.940	0.944	0.180
w/o HOC	0.899	0.689	0.937	0.945	0.181
w/o CG	0.906	0.687	0.945	0.948	0.179
w/o DM	0.901	0.690	0.939	0.941	0.180
+ KP	0.891	0.691	0.940	0.943	0.183
<b>SCAR (our)</b>	<b>0.916</b>	<b>0.698</b>	<b>0.951</b>	<b>0.954</b>	<b>0.187</b>

egory (highlighted in green) substitutes our proposed representation with existing representations, including optical flow (OF), hand-object masks (HOM), and depth maps (DM). As shown in Tab. 2, these representations, which capture only one aspect of the interaction, lead to reduced performance. For instance, the OF and DM variants fail spatiotemporal coherence, causing objects (e.g., the blue ruler) to disappear, while the HOM variant lacks explicit contact cues, leading to missed grasps (see supplementary material for qualitative comparison).

**Ablation Study on Proposed Representation.** The second category (highlighted in yellow) consists of variants ablating our proposed components: w/o HOC (removing hand-object contours), w/o CG (removing contact region), w/o

DM (removing depth maps), and +KP (adding rendered 2D hand keypoints). As shown in Tab. 2, removing any of our core components (w/o HOC, w/o CG, w/o DM) degrades performance, confirming their complementary importance. The qualitative comparison (see supplementary material) reveals that variants lacking spatial localization (w/o HOC) or holistic structure (w/o DM) struggle with object consistency, and the w/o CG variant fails fine-grained tasks (e.g., measuring cup). Furthermore, adding 2D keypoints (+KP) also degrades performance, as an overly complex auxiliary generative target hinders optimization.

In summary, compared with the above existing representations and our ablated variants, our SCAR achieves the best quantitative metrics shown in Tab. 2 and generates more physically realistic videos (see the supplementary material). This demonstrates that our HOI representation benefits from a more comprehensive and interaction-oriented supervisory signal, which effectively guides the learning of fine-grained interaction physics.

## 5. Conclusion

In this work, we introduce an open-world hand-object interaction video generation framework based on a structure and contact-aware representation. We introduce a novel HOI representation that encodes hand-object contact, the spatial localization of the hand and object, and the holistic structure of the observed scene. This representation is leveraged within a joint-generation paradigm featuring a share-and-specialization strategy that mitigates the error accumulation of prior multi-stage methods. We further

curate the above representation for more than 100K HOI videos to enable large-scale training. Experiments demonstrate that our method substantially outperforms prior work in physical realism and temporal consistency, and strong generalization to challenging open-world scenarios.

## References

- [1] Shuai Bai, Kebin Chen, Xuejing Liu, Jialin Wang, Wenbin Ge, Sibo Song, Kai Dang, Peng Wang, Shijie Wang, Jun Tang, et al. Qwen2. 5-vl technical report. *arXiv preprint arXiv:2502.13923*, 2025. [2](#), [3](#)
- [2] Chen Bao, Jiarui Xu, Xiaolong Wang, Abhinav Gupta, and Homanga Bharadhwaj. Handsonvlm: Vision-language models for hand-object interaction prediction. *arXiv preprint arXiv:2412.13187*, 2024. [3](#)
- [3] Andreas Blattmann, Tim Dockhorn, Sumith Kulal, Daniel Mendelevitch, Maciej Kilian, Dominik Lorenz, Yam Levi, Zion English, Vikram Voleti, Adam Letts, et al. Stable video diffusion: Scaling latent video diffusion models to large datasets. *arXiv preprint arXiv:2311.15127*, 2023. [3](#)
- [4] Junuk Cha, Jihyeon Kim, Jae Shin Yoon, and Seungryul Baek. Text2hoi: Text-guided 3d motion generation for hand-object interaction. In *Proceedings of the IEEE/CVF Conference on Computer Vision and Pattern Recognition*, pages 1577–1585, 2024. [2](#)
- [5] Sili Chen, Hengkai Guo, Shengnan Zhu, Feihu Zhang, Zilong Huang, Jiashi Feng, and Bingyi Kang. Video depth anything: Consistent depth estimation for super-long videos. In *Proceedings of the Computer Vision and Pattern Recognition Conference*, pages 22831–22840, 2025. [2](#), [4](#)
- [6] Lingwei Dang, Ruizhi Shao, Hongwen Zhang, Wei Min, Yebin Liu, and Qingyao Wu. Svimo: Synchronized diffusion for video and motion generation in hand-object interaction scenarios. *arXiv preprint arXiv:2506.02444*, 2025. [2](#)
- [7] Hehe Fan, Tao Zhuo, Xin Yu, Yi Yang, and Mohan Kankanhalli. Understanding atomic hand-object interaction with human intention. *IEEE Transactions on Circuits and Systems for Video Technology*, 32(1):275–285, 2021. [2](#)
- [8] Yingying Fan, Quanwei Yang, Kaisiyuan Wang, Hang Zhou, Yingying Li, Haocheng Feng, Errui Ding, Yu Wu, and Jingdong Wang. Re-hold: Video hand object interaction reenactment via adaptive layout-instructed diffusion model. In *Proceedings of the Computer Vision and Pattern Recognition Conference*, pages 17550–17560, 2025. [3](#)
- [9] Qijun Gan, Yi Ren, Chen Zhang, Zhenhui Ye, Pan Xie, Xiang Yin, Zehuan Yuan, Bingyue Peng, and Jianke Zhu. Humandit: Pose-guided diffusion transformer for long-form human motion video generation. *arXiv preprint arXiv:2502.04847*, 2025. [3](#)
- [10] Patrick Grady, Chengcheng Tang, Christopher D Twigg, Minh Vo, Samarth Brahmbhatt, and Charles C Kemp. Contactopt: Optimizing contact to improve grasps. In *Proceedings of the IEEE/CVF Conference on Computer Vision and Pattern Recognition*, pages 1471–1481, 2021. [2](#)
- [11] Abhinav Gupta, Aniruddha Kembhavi, and Larry S Davis. Observing human-object interactions: Using spatial and functional compatibility for recognition. *IEEE transactions on pattern analysis and machine intelligence*, 31(10):1775–1789, 2009. [2](#)
- [12] Jonathan Ho, Ajay Jain, and Pieter Abbeel. Denoising diffusion probabilistic models. *Advances in neural information processing systems*, 33:6840–6851, 2020. [5](#)
- [13] Wenyi Hong, Ming Ding, Wendi Zheng, Xinghan Liu, and Jie Tang. Cogvideo: Large-scale pretraining for text-to-video generation via transformers. In *The Eleventh International Conference on Learning Representations*, 2023. [2](#)
- [14] Edward J Hu, Yelong Shen, Phillip Wallis, Zeyuan Allen-Zhu, Yuanzhi Li, Shean Wang, Lu Wang, Weizhu Chen, et al. Lora: Low-rank adaptation of large language models. *ICLR*, 1(2):3, 2022. [5](#)
- [15] Hezhen Hu, Weilun Wang, Wengang Zhou, and Houqiang Li. Hand-object interaction image generation. *Advances in Neural Information Processing Systems*, 35:23805–23817, 2022. [2](#)
- [16] Yucheng Hu, Yanjiang Guo, Pengchao Wang, Xiaoyu Chen, Yen-Jen Wang, Jianke Zhang, Koushil Sreenath, Chaochao Lu, and Jianyu Chen. Video prediction policy: A generalist robot policy with predictive visual representations. In *Forty-second International Conference on Machine Learning*, 2025. [2](#), [3](#)
- [17] Mingzhen Huang, Fu-Jen Chu, Bugra Tekin, Kevin J Liang, Haoyu Ma, Weiyao Wang, Xingyu Chen, Pierre Gleize, Hongfei Xue, Siwei Lyu, et al. Hoigpt: Learning long-sequence hand-object interaction with language models. In *Proceedings of the Computer Vision and Pattern Recognition Conference*, pages 7136–7146, 2025. [2](#)
- [18] Ziqi Huang, Yinan He, Jiashuo Yu, Fan Zhang, Chenyang Si, Yuming Jiang, Yuanhan Zhang, Tianxing Wu, Qingyang Jin, Nattapol Chanpaisit, et al. Vbench: Comprehensive benchmark suite for video generative models. In *Proceedings of the IEEE/CVF Conference on Computer Vision and Pattern Recognition*, pages 21807–21818, 2024. [5](#), [6](#)
- [19] Hanwen Jiang, Shaowei Liu, Jiashun Wang, and Xiaolong Wang. Hand-object contact consistency reasoning for human grasps generation. In *Proceedings of the IEEE/CVF international conference on computer vision*, pages 11107–11116, 2021. [2](#)
- [20] Wonjoon Jin, Qi Dai, Chong Luo, Seung-Hwan Baek, and Sunghyun Cho. Flovd: Optical flow meets video diffusion model for enhanced camera-controlled video synthesis. In *Proceedings of the Computer Vision and Pattern Recognition Conference*, pages 2040–2049, 2025. [2](#), [3](#), [6](#), [7](#), [8](#)
- [21] Jaeyeon Kang, Seoung Wug Oh, and Seon Joo Kim. Error compensation framework for flow-guided video inpainting. In *European conference on computer vision*, pages 375–390. Springer, 2022. [2](#)
- [22] Korrawe Karunratanakul, Jinlong Yang, Yan Zhang, Michael J Black, Krikamol Muandet, and Siyu Tang. Grasping field: Learning implicit representations for human grasps. In *2020 International Conference on 3D Vision (3DV)*, pages 333–344. IEEE, 2020. [2](#)
- [23] Weijie Kong, Qi Tian, Zijian Zhang, Rox Min, Zuozhuo Dai, Jin Zhou, Jiangfeng Xiong, Xin Li, Bo Wu, Jianwei Zhang,

et al. Hunyuandvideo: A systematic framework for large video generative models. *arXiv preprint arXiv:2412.03603*, 2024. 3

[24] Gen Li, Bo Zhao, Jianfei Yang, and Laura Sevilla-Lara. Mask2iv: Interaction-centric video generation via mask trajectories. *arXiv preprint arXiv:2510.03135*, 2025. 2, 3

[25] Shaowei Liu, Yang Zhou, Jimei Yang, Saurabh Gupta, and Shenlong Wang. Contactgen: Generative contact modeling for grasp generation. In *Proceedings of the IEEE/CVF International Conference on Computer Vision*, pages 20609–20620, 2023. 2

[26] Shilong Liu, Zhaoyang Zeng, Tianhe Ren, Feng Li, Hao Zhang, Jie Yang, Qing Jiang, Chunyuan Li, Jianwei Yang, Hang Su, et al. Grounding dino: Marrying dino with grounded pre-training for open-set object detection. In *European conference on computer vision*, pages 38–55. Springer, 2024. 4

[27] Xingchao Liu, Chengyue Gong, and qiang liu. Flow straight and fast: Learning to generate and transfer data with rectified flow. In *The Eleventh International Conference on Learning Representations*, 2023. 5

[28] Yun Liu, Haolin Yang, Xu Si, Ling Liu, Zipeng Li, Yuxiang Zhang, Yebin Liu, and Li Yi. Taco: Benchmarking generalizable bimanual tool-action-object understanding. In *Proceedings of the IEEE/CVF Conference on Computer Vision and Pattern Recognition*, pages 21740–21751, 2024. 5, 6, 7

[29] Hao Luo, Yicheng Feng, Wanpeng Zhang, Sipeng Zheng, Ye Wang, Haoqi Yuan, Jiazheng Liu, Chaoyi Xu, Qin Jin, and Zongqing Lu. Being-h0: vision-language-action pre-training from large-scale human videos. *arXiv preprint arXiv:2507.15597*, 2025. 2

[30] Youxin Pang, Ruizhi Shao, Jiajun Zhang, Hanzhang Tu, Yun Liu, Boyao Zhou, Hongwen Zhang, and Yebin Liu. Manivideo: Generating hand-object manipulation video with dexterous and generalizable grasping. In *Proceedings of the Computer Vision and Pattern Recognition Conference*, pages 12209–12219, 2025. 2, 3

[31] William Peebles and Saining Xie. Scalable diffusion models with transformers. In *Proceedings of the IEEE/CVF international conference on computer vision*, pages 4195–4205, 2023. 3

[32] Siyou Pei, Alexander Chen, Jaewook Lee, and Yang Zhang. Hand interfaces: Using hands to imitate objects in ar/vr for expressive interactions. In *Proceedings of the 2022 CHI conference on human factors in computing systems*, pages 1–16, 2022. 2

[33] Nikhila Ravi, Valentin Gabeur, Yuan-Ting Hu, Ronghang Hu, Chaitanya Ryali, Tengyu Ma, Haitham Khedr, Roman Rädel, Chloe Rolland, Laura Gustafson, Eric Mintun, Junting Pan, Kalyan Vasudev Alwala, Nicolas Carion, Chao-Yuan Wu, Ross Girshick, Piotr Dollar, and Christoph Feichtenhofer. SAM 2: Segment anything in images and videos. In *The Thirteenth International Conference on Learning Representations*, 2025. 2, 4

[34] Weiming Ren, Huan Yang, Ge Zhang, Cong Wei, Xinrun Du, Wenhao Huang, and Wenhui Chen. Consisti2v: Enhancing visual consistency for image-to-video generation. *Transactions on Machine Learning Research*, 2024. 2

[35] Javier Romero, Dimitrios Tzionas, and Michael J. Black. Embodied hands: Modeling and capturing hands and bodies together. *ACM Transactions on Graphics, (Proc. SIGGRAPH Asia)*, 36(6), 2017. 2

[36] Xiaoyu Shi, Zhaoyang Huang, Fu-Yun Wang, Weikang Bian, Dasong Li, Yi Zhang, Manyuan Zhang, Ka Chun Cheung, Simon See, Hongwei Qin, et al. Motion-i2v: Consistent and controllable image-to-video generation with explicit motion modeling. In *ACM SIGGRAPH 2024 Conference Papers*, pages 1–11, 2024. 2, 3

[37] Team Wan, Ang Wang, Baole Ai, Bin Wen, Chaojie Mao, Chen-Wei Xie, Di Chen, Feiwu Yu, Haiming Zhao, Jianxiao Yang, et al. Wan: Open and advanced large-scale video generative models. *arXiv preprint arXiv:2503.20314*, 2025. 2, 3, 6, 7, 8

[38] Jing Wang, Fengzhuo Zhang, Xiaoli Li, Vincent YF Tan, Tianyu Pang, Chao Du, Aixin Sun, and Zhuoran Yang. Error analyses of auto-regressive video diffusion models: A unified framework. *arXiv preprint arXiv:2503.10704*, 2025. 2

[39] Luozhou Wang, Yijun Li, Zhifei Chen, Jui-Hsien Wang, Zhifei Zhang, He Zhang, Zhe Lin, and Ying-Cong Chen. Transpixeler: Advancing text-to-video generation with transparency. In *Proceedings of the Computer Vision and Pattern Recognition Conference*, pages 18229–18239, 2025. 2, 3

[40] Lizhen Wang, Zhurong Xia, Tianshu Hu, Pengrui Wang, Pengfei Wei, Zerong Zheng, Ming Zhou, Yuan Zhang, and Mingyuan Gao. Dreamactor-h1: High-fidelity human-product demonstration video generation via motion-designed diffusion transformers. *arXiv preprint arXiv:2506.10568*, 2025. 3

[41] Jason Wei, Xuezhi Wang, Dale Schuurmans, Maarten Bosma, Fei Xia, Ed Chi, Quoc V Le, Denny Zhou, et al. Chain-of-thought prompting elicits reasoning in large language models. *Advances in neural information processing systems*, 35:24824–24837, 2022. 2

[42] Ziyi Xu, Ziyao Huang, Juan Cao, Yong Zhang, Xiaodong Cun, Qing Shuai, Yuchen Wang, Linchao Bao, Jintao Li, and Fan Tang. Anchorcrafter: Animate cyberanchors saling your products via human-object interacting video generation. *arXiv preprint arXiv:2411.17383*, 2024. 3

[43] Zhuoyi Yang, Jiayan Teng, Wendi Zheng, Ming Ding, Shiyu Huang, Jiazheng Xu, Yuanming Yang, Wenyi Hong, Xiaohan Zhang, Guanyu Feng, Da Yin, Yuxuan Zhang, Weihai Wang, Yean Cheng, Bin Xu, Xiaotao Gu, Yuxiao Dong, and Jie Tang. Cogvideox: Text-to-video diffusion models with an expert transformer. In *The Thirteenth International Conference on Learning Representations*, 2025. 2, 3, 6, 7, 8

[44] Guy Yariv, Yuval Kirstain, Amit Zohar, Shelly Sheynin, Yaniv Taigman, Yossi Adi, Sagie Benaim, and Adam Polyak. Through-the-mask: Mask-based motion trajectories for image-to-video generation. In *Proceedings of the Computer Vision and Pattern Recognition Conference*, pages 18198–18208, 2025. 2, 3

[45] Hongxiang Zhao, Xingchen Liu, Mutian Xu, Yiming Hao, Weikai Chen, and Xiaoguang Han. Taste-rob: Advancing video generation of task-oriented hand-object interaction for generalizable robotic manipulation. In *Proceedings of the*

*Computer Vision and Pattern Recognition Conference*, pages 27683–27693, 2025. [2](#), [3](#), [5](#), [6](#), [7](#)

[46] Bohan Zhou, Yi Zhan, Zhongbin Zhang, and Zongqing Lu. Megohand: Multimodal egocentric hand-object interaction motion generation. *arXiv preprint arXiv:2505.16602*, 2025. [2](#)

[47] Keyang Zhou, Bharat Lal Bhatnagar, Jan Eric Lenssen, and Gerard Pons-Moll. Toch: Spatio-temporal object-to-hand correspondence for motion refinement. In *European Conference on Computer Vision*, pages 1–19. Springer, 2022. [2](#)